

UNRAVELING THE NATURE OF THE NUCLEAR TRANSIENT AT2020ADPI

PAARMITA PANDEY ^{1,2}, JASON T. HINKLE ³, CHRISTOPHER S. KOCHANEK ^{1,2}, MICHAEL A. TUCKER ^{1,2}, MARK T. REYNOLDS ^{1,4},
JACK M. M. NEUSTADT ⁵, TODD A. THOMPSON ^{1,2,6}, KATIE AUCHETTL ^{7,8}, BENJAMIN. J. SHAPPEE ³, AARON DO ⁹,
DHVANIL D. DESAI ³, W. B. HOOGEN DAM ^{3,a}, C. ASHALL ³, THOMAS B. LOWE ³, MELISSA SHAHBANDEH ^{5,10} AND
ANNA V. PAYNE ¹⁰

¹Department of Astronomy, The Ohio State University, 140 W. 18th Ave., Columbus, OH 43210, USA

²Center for Cosmology and Astroparticle Physics, The Ohio State University, 191 W. Woodruff Ave., Columbus, OH 43210, USA

³Institute for Astronomy, University of Hawai'i at Manoa, 2680 Woodlawn Dr., Hawai'i, HI 96822, USA

⁴Department of Astronomy, University of Michigan, 1085 S. University Ave., Ann Arbor, MI 48109, USA

⁵Department of Physics and Astronomy, Bloomberg Center, Johns Hopkins University, Baltimore, MD 21218, USA

⁶Department of Physics, The Ohio State University, 191 W. Woodruff Ave, Columbus, OH 43210, USA

⁷School of Physics, The University of Melbourne, Parkville, VIC 3010, Australia.

⁸Department of Astronomy and Astrophysics, University of California, Santa Cruz, CA 95064, USA

⁹Institute of Astronomy and Kavli Institute for Cosmology, University of Cambridge, Madingley Road, Cambridge CB3 0HA, UK

¹⁰Space Telescope Science Institute, 3700 San Martin Drive, Baltimore, MD 21218, USA

^aNSF Graduate Research Fellow

Version September 5, 2025

ABSTRACT

Transient events associated with supermassive black holes provide rare opportunities to study accretion and the environments of supermassive black holes. We present a multiwavelength study of AT2020adpi (ZTF20acvfrag), a luminous optical/UV transient in the nucleus of the galaxy WISEA J231853.77–103505.6 ($z = 0.26$) that exhibits the properties of an ambiguous nuclear transient. Near peak, its spectral energy distribution is well described by a power law ($\lambda L_\lambda \propto \lambda^{-\alpha}$, $\alpha = 0.44 \pm 0.04$), with a maximum g -band luminosity of $(3.6 \pm 0.6) \times 10^{44}$ erg s⁻¹, which is consistent with luminous AGN flares. We detect a strong mid-infrared flare ($L_{\text{peak}}^{\text{MIR}} = (2.3 \pm 0.05) \times 10^{44}$ erg s⁻¹) delayed by ~ 240 rest-frame days, indicating a hot dust echo from material at ~ 0.2 pc. The optical and near-infrared spectra show broad H, He I, O III lines, as well as narrow Fe II, and prominent Mg II, which is a combination not typical of TDEs. Taken together, these features suggest AT2020adpi is an ambiguous nuclear transient, where an accretion episode was triggered by stellar disruption of an accretion disk or instabilities within an active nucleus. This source demonstrates the need for careful multiwavelength analysis to distinguish between extreme AGN variability and TDEs.

1. INTRODUCTION

Active galactic nuclei (AGNs) are known to vary in both their photometric brightness and spectroscopic features. This variability is primarily due to changes in the rate at which material is accreted onto the central supermassive black hole (SMBH), although variable obscuration may also play a role. While AGN variability has been studied for decades (e.g., [Andrillat 1968](#); [Tohline & Osterbrock 1976](#); [Oknyanskij 1978](#); [Padovani et al. 2017](#); [Paolillo & Papadakis 2025](#)), recent observations have revealed a broader range of events that differ significantly from the typical, low-amplitude, stochastic fluctuations commonly seen in AGN (e.g., [MacLeod et al. 2012](#); [Komossa et al. 2024](#)).

Among the most intriguing of these are changing-look AGN (e.g., [Bianchi et al. 2005](#); [Shappee et al. 2014](#); [MacLeod et al. 2016](#); [Trakhtenbrot et al. 2019b](#); [MacLeod et al. 2019](#); [Sheng et al. 2017](#); [Ricci & Trakhtenbrot 2023](#); [Guo et al. 2025](#)), where broad emission lines appear or disappear on timescales ranging from months to years. Similarly, rapid turn-on events, including changing-look low-ionization nuclear emission regions (LINERs; e.g., [Gezari et al. 2017a](#); [Yan et al. 2019](#); [Frederick et al. 2019](#)), involve a previously inactive or weakly active galactic nucleus suddenly transitioning to an AGN-like state. In addition, other transient phenomena associated with SMBHs have been identified that do not easily fit into existing classification schemes (e.g., [Kankare et al. 2017](#); [Tadhunter](#)

[et al. 2017](#); [Gromadzki et al. 2019](#); [Trakhtenbrot et al. 2019a](#); [Sheng et al. 2020](#)).

Another important class of SMBH-driven transients is Tidal Disruption Events (TDEs). These occur when a star passes too close to a SMBH and is torn apart by its tidal forces ([Rees 1988](#); [Phinney 1989](#); [Evans & Kochanek 1989](#)). A fraction of the disrupted stellar material is then accreted onto the black hole, generating a luminous transient that emits in the optical, ultraviolet, and, sometimes, radio and X-rays, gradually fading over time. The characteristics of these events depend on several factors: the orbital parameters of the disrupted star ([Guillochon & Ramirez-Ruiz 2013](#); [Dai et al. 2018](#)), the physical properties of both the star and the black hole ([Guillochon & Ramirez-Ruiz 2013](#); [Kochanek 2016](#)), and the effects of radiative feedback from accretion ([Gaskell & Rojas Lobos 2014](#); [Strubbe & Murray 2015](#); [Roth et al. 2016](#); [Roth & Kasen 2018](#)).

TDEs typically radiate on the order of 10^{51} erg in observable bands ([Holoien et al. 2014a](#); [Auchettl et al. 2017](#); [Mockler & Ramirez-Ruiz 2021](#)), corresponding to the conversion of less than $0.01 M_\odot$ of mass into radiation under the assumption of a 10% accretion efficiency ($\eta = 0.1$). This suggests that most bound debris is expelled rather than accreted, or that the accretion efficiency is lower than expected. However, when the emission is integrated over the years-long fading phase beyond the initial months of peak activity, the total radiated energy may approach that expected from the accretion of up

to $\sim 0.1 M_{\odot}$ (van Velzen et al. 2019).

TDEs and AGN differ markedly in their emission properties across wavelengths. Optically selected TDEs are dominated by a strong UV/optical blackbody spectral energy distribution (SED) with nearly constant temperatures of 20,000 – 50,000 K (Gezari et al. 2012; Holoien et al. 2014b; van Velzen et al. 2021), while the UV/optical SEDs of AGNs are usually best fit with power laws, $\lambda L_{\lambda} \propto \lambda^{-\alpha}$ (e.g., Vanden Berk et al. 2001; Temple et al. 2023), with $1 < \alpha < 2$ (e.g., Koratkar & Blaes 1999; Vanden Berk et al. 2001). Some TDEs emit soft X-rays (kT $\sim 30 - 60$ eV) (Holoien et al. 2016a,c; Hinkle et al. 2021b; Wevers 2020), and are typically much softer than the X-ray emission from AGN, which extends beyond 10 keV due to Comptonization (Ricci et al. 2017; Auchettl et al. 2017, 2018). TDEs generally show a rapid, luminous flare with a smooth peak and monotonic decline (Holoien et al. 2014b, 2019b; Nicholl et al. 2016; Auchettl et al. 2018; Hinkle et al. 2021b; Hammerstein et al. 2023). In contrast, AGNs exhibit stochastic variability and occasional rebrightening in flares (MacLeod et al. 2016). Moreover, TDEs typically occur on lower-mass SMBHs ($\leq 10^7 M_{\odot}$) (Mockler et al. 2023), since main-sequence stars approaching more massive black holes would pass through the event horizon without disruption (Rees 1988).

Spectroscopically, TDEs feature blue continua and broad H and/or He emission lines, often with full width at half maximum (FWHM) $\geq 10,000$ km/s, sometimes accompanied by metal lines or Bowen fluorescence (Arcavi et al. 2014; Holoien et al. 2016a,c; Blagorodnova et al. 2017; Leloudas et al. 2019a; Hammerstein et al. 2023). In contrast, AGN spectra typically display emission lines of width ~ 5000 km/s, including prominent Balmer and forbidden lines like [OIII] and [NII] (Vanden Berk et al. 2001; Frederick et al. 2020; Sheng et al. 2020). Their UV spectra also differ significantly. In particular, AGNs show strong Mg II ($\lambda 2798\text{\AA}$) emission, which is absent in TDEs (Brown et al. 2018; Hung et al. 2020a; van Velzen et al. 2021; Yao et al. 2023). The line evolution with respect to luminosity also differs; TDEs generally exhibit a positive correlation between line luminosity and line width, leading to narrower emission lines as the TDE fades (Holoien et al. 2019a; Hinkle et al. 2021a; Charalampopoulos et al. 2022), whereas AGNs show the inverse trend, where the Balmer lines broaden as AGN fades (Peterson et al. 2004; Denney et al. 2009; Shen & Kelly 2012).

The advent of wide-field, non-targeted sky surveys such as the All-Sky Automated Survey for Supernovae (ASAS-SN; Shappee et al. 2014; Kochanek et al. 2017), the Asteroid Terrestrial Impact Last Alert System (ATLAS; Tonry et al. 2018), the Zwicky Transient Facility (ZTF; Bellm et al. 2019a), the Young Supernova Experiment (Jones et al. 2021), and the Panoramic Survey Telescope and Rapid Response System (Pan-STARRS; Chambers et al. 2016) has significantly expanded the range of transient phenomena observed in galactic nuclei. This has led to increased detection of nuclear transients such as CL-AGN and TDEs, and transients whose physical origins remain ambiguous (e.g. Kankare et al. 2017; Neustadt et al. 2020; Hinkle et al. 2022a; Hinkle et al. 2025). These events have been named ambiguous nuclear transients (ANTs) since they do not fit into the known categories of standard AGN variability, TDEs, or supernovae (SNe; Wiseman et al. 2025; Hinkle 2024a). The ANTs often display peculiar features and involve substantial changes in previously steady accretion systems. These behaviors suggest

complex interactions, such as an SNe or TDE disrupting an existing AGN disk. Some recent examples include PS1-10adi (Kankare et al. 2017), ASASSN-18jd (Neustadt et al. 2020), ASASSN-18el (Trakhtenbrot et al. 2019c; Ricci et al. 2020), ASASSN-17jz (Holoien et al. 2022), AT2018dyk (Frederick et al. 2019), ASASSN-20hx (Hinkle et al. 2022b), AT2021loi (Makrygianni et al. 2023), and AT2021wx (Wiseman et al. 2023; Subrayan et al. 2023). These nuclear outbursts are most likely powered by accretion onto SMBHs, potentially offering new insight into black hole accretion processes, especially in galaxies that are otherwise dormant. A distinct subclass of ANTs, known as extreme nuclear transients (ENTs), represents the most energetic transients currently observed. These events may occur due to the tidal disruption of massive stars ($3-10 M_{\odot}$) (Hinkle et al. 2025).

In this paper, we present observations of the ANT AT2020adpi (ZTF20acvfrac/ATLAS20bjzp/Gaia21aid, RA=349.72405, Dec=-10.58495) at $z = 0.26$ (Chu et al. 2021a). This transient was first reported in Wiseman et al. (2025) as a part of a study of 11 ANTs. Further details and comparison with their analysis are detailed in Section 4. Section 2 describes the photometric and spectroscopic observations of the transient. In Section 3, we examine the properties of the host galaxy, derive the UV/optical SED, and other key characteristics of the transient. Finally, in Section 4, we discuss the nature of AT2020adpi within the broader context of TDEs, standard AGN variability, and the emerging class of ANTs. We adopt a luminosity distance of $D_L = 1360.4$ Mpc for a flat universe with $h = 0.696$, $\Omega_M = 0.286$, and $\Omega_{\Lambda} = 0.714$ (Wright 2006). We correct the photometry for a Galactic extinction of $A_V = 0.074$ mag (Schlafly & Finkbeiner 2011).

2. OBSERVATIONS AND SURVEY DATA

This section summarizes the archival data available for the host galaxy and our new photometry and spectroscopy of AT2020adpi. All the data were corrected for Galactic extinction.

2.1. Photometry

We retrieved the Zwicky Transient Facility (ZTF; Graham et al. 2019; Bellm et al. 2019b) optical light curve of AT2020adpi spanning the period from 17 March 2018 (MJD 58194) to 21 July 2025 (MJD 60877). We used the IPAC ZTF forced photometry server g , r , and i band data (Masci et al. 2023), following the recommended procedures¹. To assess any faint pre-event activity in the light curve, we computed 100-day moving averages of the difference-image fluxes relative to the reference image, to search for any low-level variability. We also used the publicly available optical photometry from Gaia Data Release 3 (DR3; Gaia Collaboration et al. 2021). We used W1 and W2 mid-infrared (MIR) data from the Wide-field Infrared Survey Explorer (WISE; Mainzer et al. 2011) for our analysis. We retrieved light curves using the method described by Hwang & Zakamska (2020). We group the data into 24-hour bins and use the median magnitude within each bin. The uncertainty is derived from the photometric error estimates.

During the period from MJD 59411 – 59455 ($\approx 30-80$ days post peak), the Neils Gehrels Swift Observatory observed the

¹ https://irsa.ipac.caltech.edu/data/ZTF/docs/ztf_forced_photometry.pdf

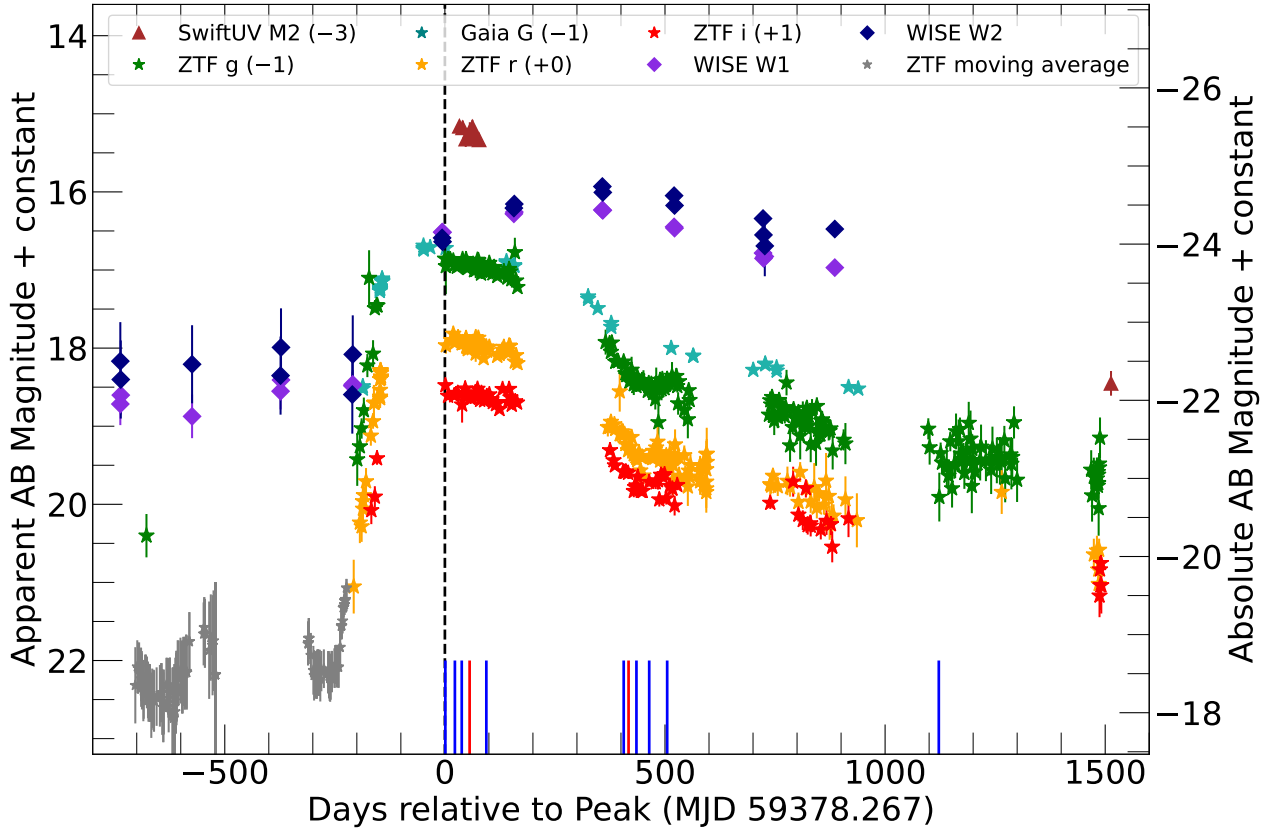


FIG. 1.— Host-subtracted UV, optical, and IR light curves of AT2020adpi, showing the Swift UVM2 band, ZTF g, r, i bands, Gaia G band, and WISE W1 and W2 bands. The photometry spans from roughly 800 days before peak (MJD = 59378.267) to roughly 1500 days after peak in observer-frame days. The gray ZTF points are the 100-day moving average of the pre-event ZTF fluxes. The blue (red) bars along the time axis show the epochs of optical (near-IR) spectroscopic follow-up. The black line is the adopted time reference. All data are corrected for Galactic extinction and are in the AB magnitude system, including the WISE data. The light curves have been offset for visual clarity.

transient using all six ultraviolet and optical (UVOT) (Poole et al. 2008) filters: V (5468 Å), B (4392 Å), U (3465 Å), $UVW1$ (2600 Å), $UVM2$ (2246 Å), and $UVW2$ (1928 Å) for ~ 2500 s. We also requested a Swift target of opportunity observations with the UVM2 filter for the UVOT and XRT for 4 kiloseconds in July 2025, approximately 1500 days post-peak brightness. For each epoch, two exposures were obtained for each filter. These were combined into single images using the HEASoft utility `uvotimsum`. Source counts were then extracted using `uvotsource` with a circular aperture of radius $5''.0$ centered on the transient. Background counts were measured from a nearby, source-free region with a radius of $\sim 50''.0$. The resulting count rates were converted into physical fluxes and magnitudes using HEASoft *version 6.34* and the CALDB release 2024-08-12_V6.34 (Poole et al. 2008; Breeveld et al. 2010).

Figure 1 shows the UV/optical/mid-IR light curves of AT2020adpi. We only show the Swift UVM2 band of the UVOT filters. We chose MJD 59378.267 as the reference epoch for our light curve and spectral parameters; the reason for choosing this epoch is described in Section 3.4. The gray data points are 100-day moving averages of the ZTF fluxes.

They suggest a small jump in flux starting roughly about two years before peak, possibly with a small flare prior to the transient.

The Swift XRT observed the transient simultaneously with the UVOT. No X-ray emission was detected either near peak (total exposure of 9.4 ks), at late times (4.0 ks), or in the combined 13.4 ks dataset. We derive 3σ upper limits on the X-ray flux incorporating the first set of observations near peak (9.4 ks), 1500 days post peak (4 ks), and the total time of 13.4 ks, assuming a power-law model $dN/dE \propto E^{-\gamma}$, with $\gamma = 1.8$ typical for AGN spectra, and a hydrogen column density of $N_H = 0.024 \times 10^{22} \text{ cm}^{-2}$ (Dickey & Lockman 1990; Kalberla et al. 2005; HI4PI Collaboration et al. 2016). For the near-peak observations, we get $f_X < 6.9 \times 10^{-14} \text{ erg s}^{-1} \text{ cm}^{-2}$ in the 0.5–10.0 keV band, corresponding to $L_X \leq 1.4 \times 10^{43} \text{ erg s}^{-1}$. The most recent observations, we constrained $f_X < 2.0 \times 10^{-12} \text{ erg s}^{-1} \text{ cm}^{-2}$ (0.5–10.0 keV), and $L_X \leq 4.2 \times 10^{44} \text{ erg s}^{-1}$. Overall, for the combined set of observations, we have $f_X < 6.3 \times 10^{-14} \text{ erg s}^{-1} \text{ cm}^{-2}$ in the 0.5–10.0 keV band, corresponding to $L_X \leq 1.3 \times 10^{43} \text{ erg s}^{-1}$.

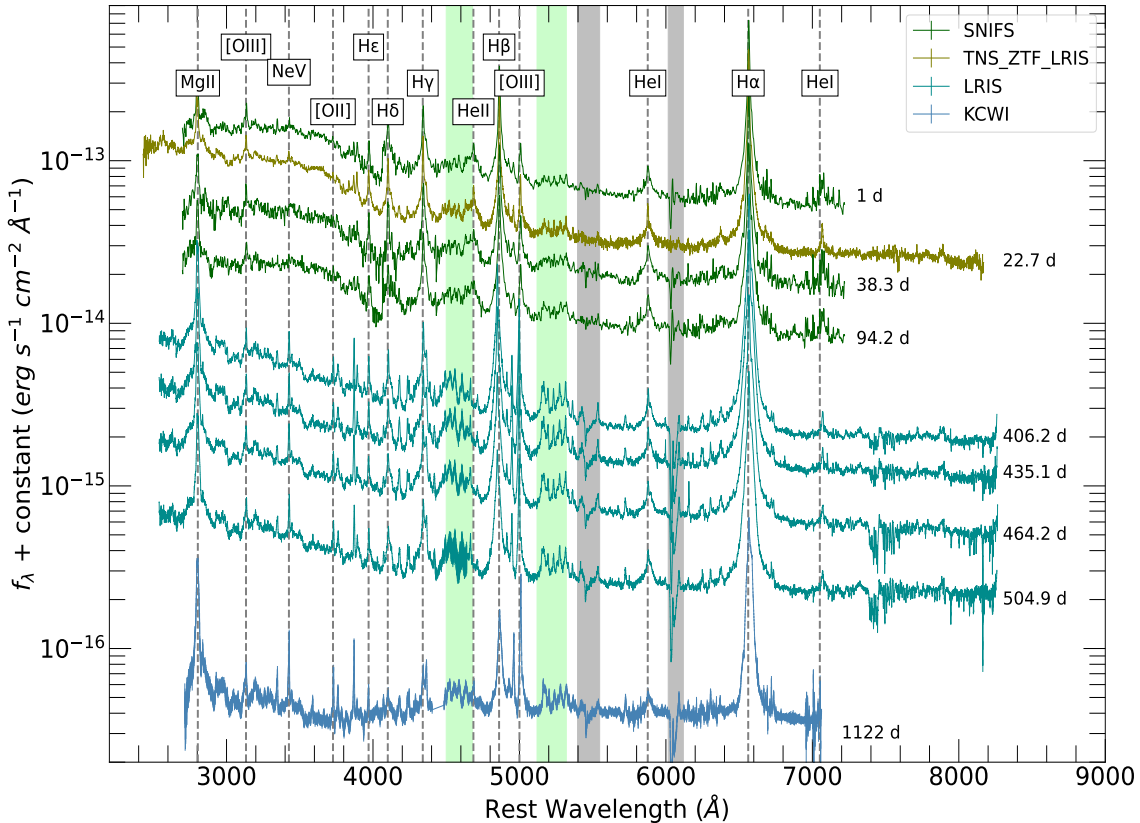


FIG. 2.— SNIFS, LRIS, and KCWI optical spectra of AT2020adpi, where the time after peak in the observed frame is to the right of each spectrum. The spectra span from almost 1 day after peak UV/optical emission (top) until 1122 days after peak (bottom). Prominent emission lines are labeled. The green shaded region highlights the Fe II emission complex. The gray shaded regions show the telluric bands. The spectra are offset for visibility.

2.2. Spectroscopic Observations

We obtained spectroscopic observations of AT2020adpi from several sources. The three spectra from the SuperNova Integral Field Spectrograph (SNIFS; Lantz et al. 2004) on the 88-inch University of Hawaii’s telescope (UH88) were obtained near peak and between 30 – 100 days post flare. We obtained spectra from the Keck Low-Resolution Imaging Spectrometer (LRIS; Oke et al. 1995) on the 10-m Keck I telescope more than a year after the optical peak. Finally, we obtained a spectrum of AT2020adpi with KCWI on Keck in July 2024 (MJD 60500) when it had nearly faded to the pre-flare level. We also used the TNS spectrum from ZTF taken ~ 20 days after the peak (Chu et al. 2021b).

The optical spectra from SNIFS were calibrated and reduced using the SCAT pipeline (Tucker et al. 2022). LRIS spectra were reduced with PyPeIt (Prochaska et al. 2020b; Prochaska et al. 2020c; Prochaska et al. 2020a). KCWI spectra were reduced with KCWI DRP². An initial flux calibration was performed using spectrophotometric standard stars observed on the same nights as the science targets. Figure 2 shows the optical spectroscopic evolution of AT2020adpi spanning from the peak UV/optical emission time to ~ 1100 days post-peak in the observer’s frame.

² <https://kcwi-drp.readthedocs.io/en/latest/index.html>

In addition, we acquired two near-infrared (NIR) spectra of AT2020adpi using the SpeX (Rayner et al. 2003) on the NASA Infrared Telescope Facility (IRTF). The observations were taken in prism mode with $R \sim 80$ since the source was faint for IRTF. These NIR spectra were reduced using SpeXtool (Cushing et al. 2004). Due to an overexposed calibration standard on the night of observation, the spectrum taken 56 days post-peak was re-reduced using a standard from a different night at a similar airmass. This improved the overall spectral shape, but the residuals in the telluric bands are large. Figure 3 shows the spectroscopic evolution of AT2020adpi in the near IR.

3. RESULTS

In this section, we summarize the results obtained from the host galaxy analysis, optical spectra, SED models of AT2020adpi, and the light curve.

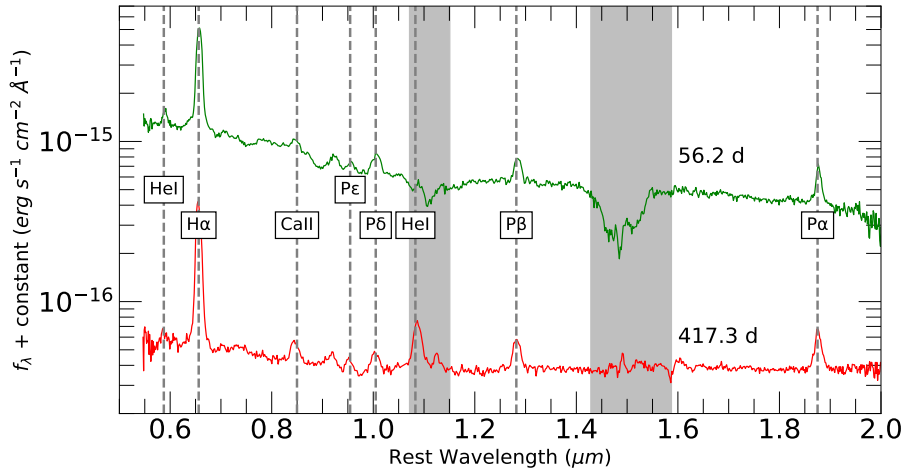


FIG. 3.— SpeX near-IR Spectra of AT2020adpi, where the time after peak in the observed frame is given above the spectra. Prominent emission lines are labeled. The vertical gray bands mark atmospheric telluric features. Due to an overexposed calibration standard on the night of the first observation, the spectrum taken at 56 days post-peak (green) was re-reduced using a standard from a different night at a similar airmass. This improved the overall spectral shape, but left large residuals in the telluric bands.

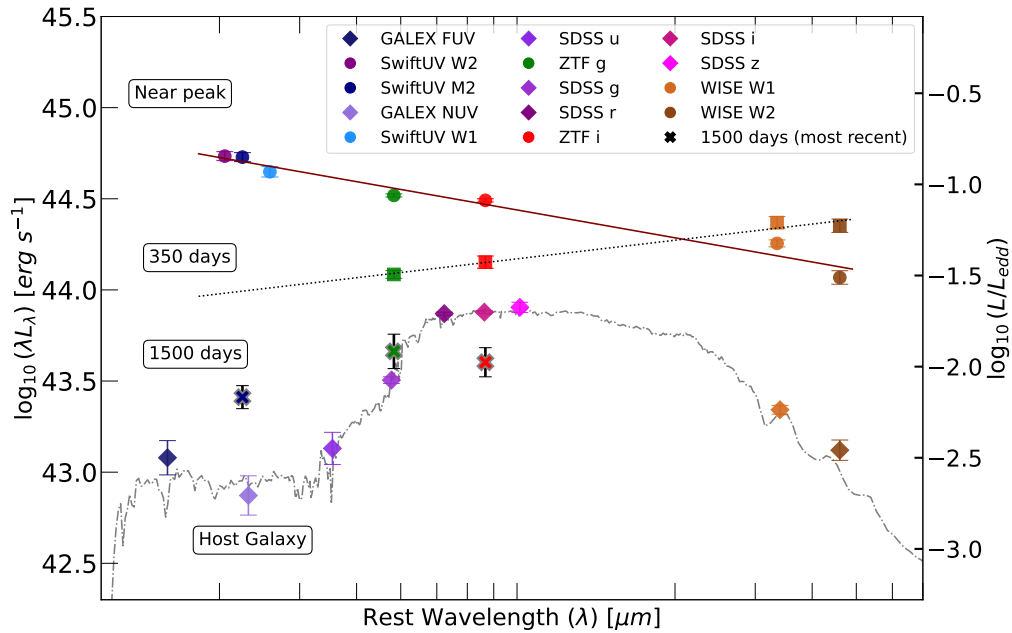


FIG. 4.— SEDs of the host galaxy and AT2020adpi near peak, 350 days and 1500 days post-peak. The FAST SED model is shown for the host and power-law fits $\lambda L_\lambda \propto \lambda^{-\alpha}$ for AT2020adpi, with $\alpha = 0.44 \pm 0.04$ near peak and $\alpha = -0.29 \pm 0.05$ at 350 days post peak. The Eddington luminosity is also indicated on the secondary y-axis, showing that the peak luminosity reaches approximately 15% of the Eddington limit.

3.1. Host Galaxy

To characterize the properties of the host galaxy, we fit the pre-transient SED using Fitting and Assessment of Synthetic Templates (FAST++; Kriek et al. 2009) to model the archival photometric measurements. We modeled the data from GALEX, SDSS, and WISE data, summarized in Table 1. We used a Cardelli et al. (1989) extinction law with a total-to-selective extinction ratio of $R_V = 3.1$, a Salpeter initial mass function (Salpeter 1955), and an exponentially declining star formation history (SFH) using Bruzual & Char-

lot (2003) models fixed at solar metallicity. The results are presented in Table 2. The host galaxy has a stellar mass of $\log(M_*/M_\odot) = 10.36^{+0.10}_{-0.07}$ and a star formation rate (SFR) of $\log(\text{SFR}/M_\odot \text{ yr}^{-1}) = -0.27^{+0.15}_{-0.13}$. Figure 4 shows the host SED with the FAST model. The SED is consistent with no current star formation due to the weak UV emission. In the model, the last burst of star-formation occurred about ~ 1 Gyr ago. Given the stellar population age and lack of current star formation, we conclude that the host is likely a post-starburst galaxy. Unfortunately, there are no pre-event spectra of the

TABLE 1
Photometric Measurements of Host Galaxy WISEA J231853.77–103505.6

Telescope and Filter	Magnitude	Magnitude Error
GALEX (AB) FUV	22.78	0.24
GALEX (AB) NUV	22.86	0.27
SDSS (AB) <i>u</i>	21.75	0.22
SDSS (AB) <i>g</i>	20.35	0.04
SDSS (AB) <i>r</i>	19.29	0.02
SDSS (AB) <i>i</i>	19.05	0.02
SDSS (AB) <i>z</i>	18.79	0.07
WISE (Vega) W1	16.08	0.06
WISE (Vega) W2	15.67	0.14
WISE (Vega) W3	11.64	0.34

TABLE 2
STELLAR POPULATION PARAMETERS FROM FAST++

Parameter	Value
Star formation timescale ($\log(\frac{\tau}{\text{yr}})$)	$8.40^{+0.06}_{-0.21}$
Stellar population age ($\log(\frac{\text{age}}{\text{yr}})$)	$9.15^{+0.05}_{-0.17}$
Dust attenuation A_V (mag)	$0.08^{+0.12}_{-0.00}$
Stellar mass ($\log M_\odot$)	$10.36^{+0.10}_{-0.07}$
Star formation rate ($\log(\frac{M_\odot}{\text{yr}})$)	$-0.27^{+0.15}_{-0.13}$
Specific star formation rate ($\log \text{yr}^{-1}$)	$-10.64^{+0.19}_{-0.17}$
Black hole mass: $\log(\frac{M_{BH}}{M_\odot})$	7.6

NOTE. — Parameters derived using FAST++ with Bruzual & Charlot (2003) templates, a Salpeter IMF, an exponentially declining SFH, and total-to-selective extinction ratio $R_V = 3.1$. The uncertainties are 68% confidence intervals. The black hole mass has been derived using a scaling relation.

host. Based on the blackhole-bulge $M_B - M_{BH}$ relation of McConnell & Ma (2013), we estimate a black hole mass of $M_{BH} \approx 10^{7.6} M_\odot$.

We also examined the light curve of the host galaxy for variability using archival data from the Catalina Real-Time Transient Survey (CRTS; Drake et al. 2009), covering the period from MJD 53710 (6 December 2005) to MJD 55398.8 (21 July 2010). No significant variability on timescales of 100 days was observed during this interval. However, the ZTF data showed a possibility of a small flare two years prior to the transient based on the 100-day moving average of the fluxes (see Fig 1).

3.2. Spectral Energy Distribution

The SED can help us distinguish the origin of the transient. In particular, AGN have power-law UV/optical SEDs while TDEs are typically well modeled by a $\sim 30,000$ K blackbody. Figure 4 shows the SED of AT2020adpi around the optical peak, 350 days post-brightening and 1500 days post-peak, as compared to the SED of the host galaxy. At peak, the SED is reasonably well fit by a $\lambda L_\lambda \propto \lambda^{-\alpha}$ power-law, with a spectral index $\alpha = 0.44 \pm 0.04$. A blackbody model is a very poor fit to the observed SED. At 350 days post-peak, we find $\alpha = -0.29 \pm 0.05$, although we have a much more limited wavelength baseline at this epoch. Thus, over the course of the first year, the SED becomes significantly redder. By integrating the observed SED at both epochs from $0.2 - 4.6 \mu\text{m}$, we estimate the partial bolometric luminosities to be $(8.9 \pm 0.3) \times 10^{44} \text{ erg s}^{-1}$ at peak and $(4.9 \pm 0.5) \times 10^{44} \text{ erg s}^{-1}$, 350 days post-peak. Those correspond to $\approx 23.5\%$ and $\approx 13\%$ of the Eddington luminosity.

The SED at 1500 days post-peak still shows a significant UV flux, almost three times higher than the host galaxy flux but roughly 3 times fainter than the extrapolation of the power-law seen at 350 days. Meanwhile, the optical flux is the same as that of the host galaxy. We also compare the UV luminosity to that of the X-ray luminosity of the source, adopting the 3σ upper limits on L_X (see Section 2.1). At early times near peak, we find $L_X/L_{UV} \leq 0.02$, while at ~ 1500 days after peak the ratio increases to $L_X/L_{UV} \leq 16.5$. For comparison, AGN typically show $L_X/L_{UV} \ll 1$ (Strateva et al. 2005), whereas TDEs often exhibit $L_X/L_{UV} \geq 1$, with jetted TDEs showing $L_X/L_{UV} \gg 1$ (Auchettl et al. 2017).

3.3. Optical Spectra

We studied the evolution of some of the strong emission lines in the optical spectra of AT2020adpi, using the `astropy.specutils` package (Earl et al. 2025) to calculate the FWHM of the emission lines. Figure 5 shows the temporal evolution of the Mg II and H α FWHM measurements for the SNIFS, LRIS, and KCWI spectra. The SNIFS data, taken at earlier epochs (1–100 days post-peak), exhibit a clear decline in line width over time as the continuum flux decreases. The LRIS data points, observed at intermediate epochs (200–300 days), appear to deviate slightly from this trend. However, this discrepancy is likely not significant, as the statistical uncertainties on the LRIS measurements are large ($\approx 250 \text{ km s}^{-1}$). The final KCWI measurement at ~ 1000 days also supports the trend of continued line narrowing at late times. The trend of emission lines narrowing as the transient fades is a characteristic of TDEs (Holoien et al. 2016a; Leloudas et al. 2019b).

The optical spectra also show coronal Fe II emission lines (highlighted by green bands in Fig 2). These lines are commonly observed in AGNs, where they arise from high-density, partially ionized gas irradiated by a strong UV/X-ray continuum (e.g., Baldwin et al. 2004; Dong et al. 2010). However, coronal Fe II emission has also been reported in a subset of TDEs, including AT2018fyk (Wevers et al. 2019a), ASASSN-15oi (Gezari et al. 2017b), and PTF-09ge (Arcavi et al. 2014). For example, Hinkle et al. (2024) shows that many galaxies that exhibit strong coronal line emission and lack typical AGN activity have similar properties to TDE host galaxies.

While the SED shows a significant decline in the UV luminosity after 350 days, the spectra (Fig 2 and 3) obtained around this epoch indicate that substantial UV radiation is still present due to the presence of the broad H and He emission lines. In fact, if the observed He I emission in the IR spectra is accurate, then its strength implies that the UV spectrum has actually hardened. The H α luminosity at peak from the SNIFS spectrum (refer to Figure 2) is $L_{H\alpha} = 5.1 \times 10^{41} \text{ erg s}^{-1}$. Assuming Case B recombination and a mean ionizing photon energy of 18 eV, we estimate an ionizing luminosity of $L_{\text{ion}} \approx 10^{43} \text{ erg s}^{-1}$. We can also use the H α /H β flux ratio (the Balmer decrement) to calculate the line-of-sight extinction. From our measured H β luminosity of $L_{H\beta} = 1.3 \times 10^{41} \text{ erg s}^{-1}$, we obtain $H\alpha/H\beta \approx 3.8$, which is larger than the intrinsic Case B value of 2.86 (Draine 2011). Assuming the line ratio is dominated by recombination, the higher observed ratio implies a color excess of $E(B - V) \approx 0.3$, with roughly 60% of the V-band flux absorbed along the line of sight.

3.4. Light Curve Analysis

We fit the ZTF *g* and Gaia *G* band light curves to try to estimate the time of optical peak. We first modeled the light

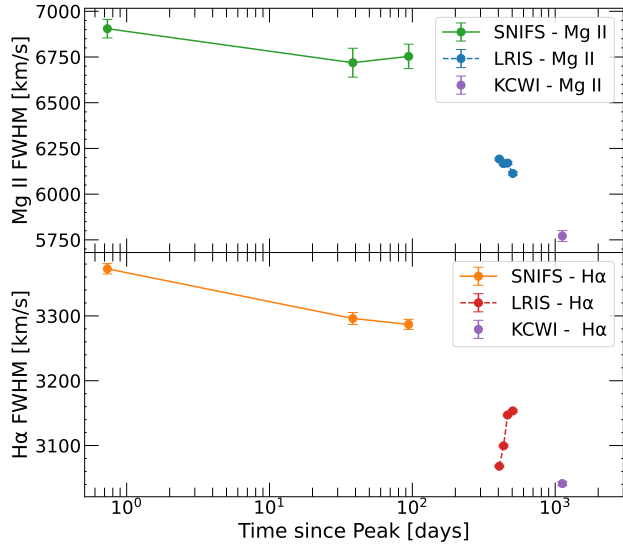


FIG. 5.— Evolution of the FWHM of Mg II and H α emission lines in the optical spectra AT2020adpi. The line width scales with the continuum flux, since as the transient fades in time, the line width decreases, which is seen in TDEs. The apparent trend in the LRIS points is just noise.

curve using an exponential function:

$$m(t) = \begin{cases} m_0 - A \cdot \exp\left(\frac{t - t_{\text{peak}}}{\tau_{\text{rise}}}\right), & \text{for } t < t_{\text{peak}} \\ m_0 - A \cdot \exp\left(-\frac{t - t_{\text{peak}}}{\tau_{\text{decay}}}\right), & \text{for } t \geq t_{\text{peak}} \end{cases} \quad (1)$$

where m_0 is the baseline magnitude, and A is the amplitude, $\tau_{\text{rise}} / \tau_{\text{decay}}$ are the rise/decay timescales. This model provides for the asymmetric shape of the light curve. Using this model, we fit $t_{\text{peak}} = \text{MJD } 59223.58 \pm 1.09$, $\tau_{\text{rise}} = 27.45 \pm 0.98$ days and $\tau_{\text{decay}} = 438.55 \pm 8.41$ days for the Gaia G band. For the ZTF g band, the values were $t_{\text{peak}} = \text{MJD } 59220.42 \pm 0.59$, $\tau_{\text{rise}} = 21.42 \pm 0.56$ days and $\tau_{\text{decay}} = 269.10 \pm 3.67$ days. All values are in the observer frame. We also simply fit a parabola to the ZTF g band. Using this procedure, we find $t_{\text{peak}} = \text{MJD } 59393.87 \pm 1.56$. Since t_{peak} is model dependent, we simply adopt the epoch of the brightest ZTF g band epoch, MJD 59378.267, as our reference time. Next, we fit the rise time of the g -band light curve as a power law with

$$L = \begin{cases} k, & \text{for } t < t_1 \text{ and} \\ k + h \left(\frac{t - t_1}{t_{\text{mid}} - t_1}\right)^\alpha, & \text{for } t \geq t_1 \end{cases} \quad (2)$$

This model fits for the baseline luminosity k , the time of first-light t_1 , a luminosity scale h , and the power-law index α . The denominator $(t_{\text{mid}} - t_1)$ normalizes the power-law term so that at $t = t_{\text{mid}}$, the luminosity is $k + h$. To reduce the number of model parameters and estimate a first-order value of α , we fix $k = 1.38 \times 10^{43} \text{ erg s}^{-1}$, the average luminosity measured over the year preceding the peak. We used the `scipy.optimize.curvefit` package to fit the model parameters. We get best-fit parameters of $t_1 = \text{MJD } 59164.77 \pm 1.44$, $h = (5.75 \pm 0.04) \times 10^{43} \text{ erg s}^{-1}$ and $\alpha = 1.86 \pm 0.07$ for the rise of AT2020adpi. The value of rise-time slope is similar to the TDEs ASASSN-19bt (Holoien et al. 2019b), ASASSN-19dj (Hinkle et al. 2021a), and ZTF19abzrhq (AT2019qiz, Nicholl et al. 2020), which all have a quadratic rise ($\alpha \simeq 2$)

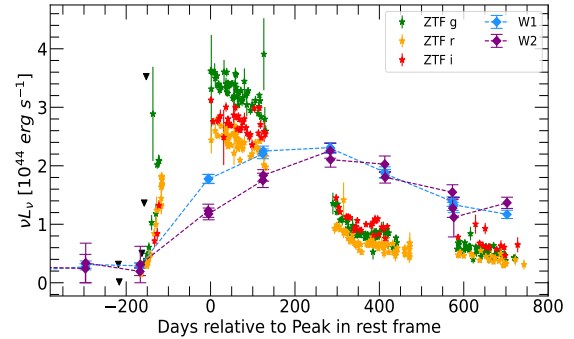


FIG. 6.— ZTF optical and WISE mid-IR light curves of AT2020pi, highlighting a significant lag, which implies the presence of a dust echo. The black triangles show the ZTF- g 3σ upper limits.

that corresponds to a “fireball” model with a photosphere expanding at constant velocity and temperature.

Based on the inferred time of first light taken from the power-law fit and the time of peak light measured from the light curve in Fig 1, we constrain the rise time to be ≈ 170 days in the rest frame. The rise time is considerably larger than that observed for the TDEs ASASSN-19bt (~ 41 days; Holoien et al. 2019d), PS18kh (~ 56 days; Holoien et al. 2019b), ASASSN-18pg (~ 54 days; Holoien et al. 2020), ASASSN-23bd (< 15 days; Hoogendam et al. 2024) and ASASSN-19dj (~ 16 days; Hinkle et al. 2021a). However, the rise time of AT2020adpi is comparable to some of the ANTs in the Wiseman et al. (2025) sample, such as AT2021lwx (198 days), AT2019kn (125 days), and AT2019brs (173 days).

In Figure 6, we see that the mid-IR light curve lags the optical light curve. In order to quantify the lag, we used JAVELIN (Zu et al. 2011) to fit the ZTF g -band and the WISE W1 light curves. JAVELIN models the continuum variability using a damped random walk (DRW) Gaussian process for interpolation, and models the second light curve (W1) as a shifted, scaled, and smoothed version of the first (g). Because the light curves are so sparse, we fixed the DRW damping timescale to $\tau_{\text{DRW}} = 200$ days (MacLeod et al. 2010, the results are not dependent on this assumption) and allowed only the amplitude σ_{DRW} to vary. Similarly, we fit only the lag time (t_{lag}) and the relative amplitude, assuming no smoothing. The light curves are too sparse to allow estimates of τ_{DRW} or to allow for an additional smoothing parameter. The best-fit lag value is $t_{\text{lag}} \approx 240.5^{+13.5}_{-47.1}$ days in the rest frame, which corresponds to $R = c \times t_{\text{lag}} \approx 0.2 \text{ pc}$.

The peak value of the optical luminosity (ZTF g) is $L_{\text{peak}}^{\text{opt}} \approx (3.6 \pm 0.6) \times 10^{44} \text{ erg s}^{-1}$, and for the MIR (WISE W1), it is $L_{\text{peak}}^{\text{MIR}} \approx (2.3 \pm 0.05) \times 10^{44} \text{ erg s}^{-1}$, making the luminosity ratio $L_{\text{MIR}}/L_{\text{opt}} \sim 0.6$. To order of magnitude, the luminosity of a dust echo from a dusty shell of radius $R \approx c \times t_{\text{lag}}$ is (Peterson 1997)

$$L_{\text{peak}}^{\text{dust}} \sim \min(1, \tau) f \frac{L_{\text{peak}}^{\text{opt}} t_{\text{peak}}}{t_{\text{lag}}}, \quad (3)$$

where t_{peak} is the duration over which the transient remains near peak luminosity, t_{lag} is the time delay of the dust echo, f is the covering fraction of the dust surrounding the source, and τ is the optical depth of the dust. Given that $L_{\text{peak}}^{\text{dust}} \sim$

TABLE 3
AGN vs. TDE PROPERTIES OF AT2020ADPI

Property	AGN/TDE-like
$\log(M_{\text{BH}}/M_{\odot}) < 8$	TDE/AGN
Fe II Emission line	AGN
Broad Mg II emission	AGN
$W1 - W2 > 0.7$ mag	AGN
Broad lines narrow as transient fades	TDE
Power-Law SED	AGN

NOTE. — Properties used to distinguish between TDEs and AGN activity, following Frederick et al. (2020); Hinkle et al. (2022b).

$L_{\text{peak}}^{\text{opt}} t_{\text{peak}}/t_{\text{lag}}$, this implies

$$\min(1, \tau) f \sim 1. \quad (4)$$

This appears to require the transient to be surrounded by dust with a high covering fraction and an optical/UV depth near or above unity. This is somewhat unexpected, as the transient exhibits a blue continuum, and the Balmer decrement suggests only $\sim 60\%$ obscuration along the line of sight. The SED also rises strongly into the UV, further suggesting low extinction in the direct viewing path beyond the Galactic contribution. This suggests that there is a considerably more UV emission at shorter wavelengths than observed by Swift, so that the pseudo-bolometric luminosity from Section 3.2 we used for L_{opt} is a significant underestimate.

4. DISCUSSION AND CONCLUSIONS

AT2020adpi is an unusual nuclear transient with properties spanning those of both optically discovered TDEs and AGN. In Table 3 we summarize the TDE-like and AGN-like features. Its total radiated energy of $(1.3 \pm 0.2) \times 10^{52}$ erg is at least an order of magnitude higher than typical supernovae and but typical for luminous TDEs and bright AGN flares. There is no evidence that it is a CL-AGN or CL-LINER, as the prominent broad emission lines (Balmer lines, Mg II, He I, etc) are present throughout the ~ 1100 days span of the optical spectra (see Fig 2).

Wiseman et al. (2025) included AT2020adpi in a sample of 11 ambiguous nuclear transients (ANTs), analyzing ZTF, ATLAS, and Pan-STARRS optical data and NEOWISE MIR light curves. They found a ~ 1 year lag between the optical and MIR peaks, consistent with our ~ 240 day rest-frame lag, and similarly identified strong Balmer emission and AGN-like features. Their estimated rise time of ~ 120 days is shorter than our ~ 166 days, likely due to observational gaps and different peak definitions. They modeled the SED with a blackbody, finding $\log(L_{\text{BB,max}}) = 44.6 \pm 0.2$ erg s^{-1} and dust temperatures of 1500–1800 K. They concluded that AT2020adpi shares traits (smooth light curve, MIR echo, strong Balmer lines) with other ANTs, possibly representing an overlap between AGN variability and massive-star TDEs.

4.1. AT2020adpi as a TDE

Several features initially suggested a TDE origin. The early-time optical/UV emission was bright and blue, similar to events like ASASSN-14li (Holoien et al. 2016a) and AT2019qiz (Hung et al. 2020b), and the optical light curve evolved smoothly without the short-timescale stochastic variability typical of AGNs (Hinkle et al. 2021b). The ~ 170 day rise is slower than most TDEs (median $\lesssim 50$ days; Hung et al.

2017), but luminous TDEs such as PS18kh (Holoien et al. 2019c) have shown extended rises.

The host galaxy is likely a post-starburst galaxy. This is, however, based only on the stellar age estimate from the SED models, and not a direct spectroscopic observation. TDEs frequently prefer post-starburst host galaxies (French et al. 2016). No prior large-amplitude variability is detected in the available archival light curves, consistent with most TDE hosts, although there may have been a small rise in flux ~ 2 years before the transient. The SMBH mass, $M_{\text{BH}} \approx 10^{7.6} M_{\odot}$, is high for TDEs (Wevers et al. 2019b), because full disruptions of main-sequence stars become rare at these masses (Rees 1988), but partial disruptions or giant-star TDEs remain possible.

The spectra, however, deviate from typical optically selected TDEs. Broad Mg II $\lambda 2798$ and prominent Fe II complexes are absent in most TDEs (Brown et al. 2018; Yao et al. 2023), but present here (Figures 2–3). Figure 7 compares AT2020adpi’s spectra with those of well-characterized TDEs and other nuclear transients. The optical spectra are similar to PS16dtm (Blanchard et al. 2017), a TDE candidate in a Narrow-line Seyfert 1, which also exhibited transient blue continuum and Fe II emission, but with a different light-curve morphology. As in many TDEs, the Balmer lines narrow as the transient fades (Holoien et al. 2019a), opposite to the trend observed in AGNs (Peterson et al. 2004).

4.2. AT2020adpi as an AGN

Several properties point toward an AGN origin. The peak SED is well fit by a power law with $\alpha = 0.44 \pm 0.04$, flatter than most quasars but within the range for Seyfert 1 AGNs (Temple et al. 2023), and inconsistent with the single-temperature blackbody typical of TDEs. The strong broad Mg II and narrow Fe II emission near $H\beta$ and [O III] are typical characteristics of Narrow-Line Seyfert 1 galaxies (Osterbrock & Pogge 1985; Wang et al. 2009).

The MIR echo peaks ~ 240 days after the optical, corresponding to a dust radius of ~ 0.2 pc, which is larger than typical TDE dust echoes (van Velzen et al. 2016) but typical of AGN dust “tori” (López-Gonzaga et al. 2016). Similarly long lags have also been reported in other ANTs (Wiseman et al. 2025). The high luminosity and a broad line region-like spectrum support the idea of a large-amplitude AGN flare.

However, typical AGN variability rarely produces such large, rapid changes. MacLeod et al. (2012) found that $|\Delta m_g| > 1$ mag in $\lesssim 150$ days occurs with a probability $\lesssim 10^{-5}$ in quasars. CL-AGNs can reach these amplitudes over months (Shappee et al. 2016; MacLeod et al. 2016), but usually show spectral evolution toward a normal AGN continuum and line ratios. Due to a lack of any pre-flare optical spectra, we cannot determine if AT2020adpi is associated with a CL-AGN.

4.3. AT2020adpi as an ANT

The combination of a smooth, luminous light curve, Balmer line narrowing, post-starburst host galaxy, power-law continuum, Mg II and Fe II emission, and a torus-scale MIR echo suggests AT2020adpi is an ANT (Wiseman et al. 2025; Hinkle 2024a). In this scenario, a TDE-like fueling episode, which can possibly be a partial stellar disruption, occurs in a galaxy with a pre-existing AGN, producing both a TDE-like response and AGN-like continuum and line features. The high dust covering fraction we infer for AT2020adpi is typical for AGNs, near the upper end values measured for ANTs

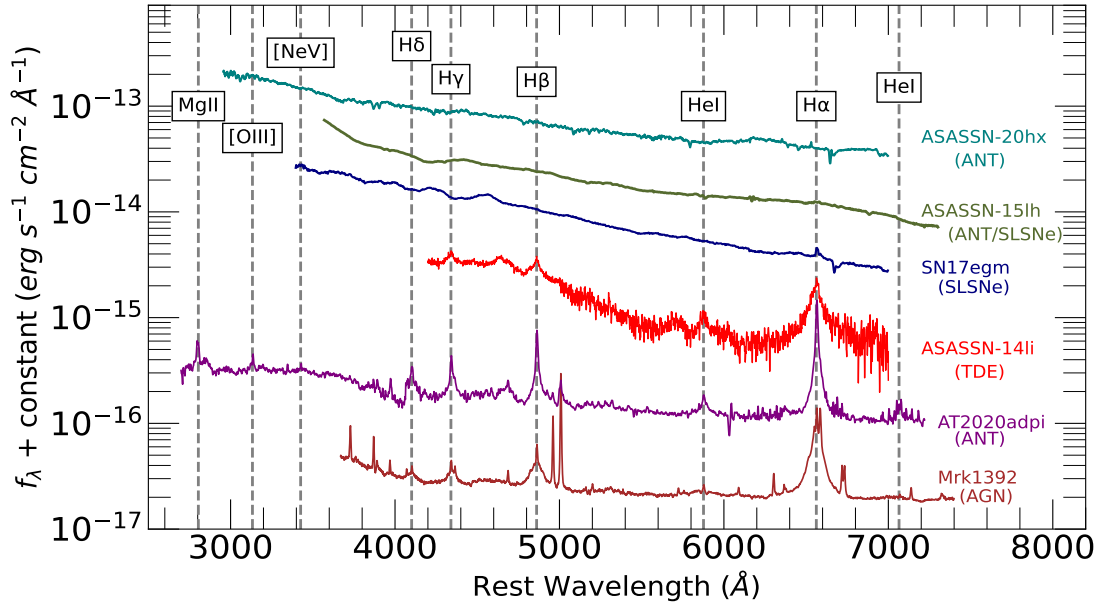


FIG. 7.— The spectrum of AT2020adpi alongside those of ANT/superluminous supernova ASASSN-15lh (Dong et al. 2016; Leloudas et al. 2016; Godoy-Rivera et al. 2017), the Type I superluminous supernova SN17egm (Bose et al. 2018), the TDE ASASSN-14li (Holoien et al. 2016b), the ANT ASASSN-20hx (Hinkle et al. 2022b), and the Seyfert 1 galaxy Mrk1392 (Adelman-McCarthy et al. 2006). All transient spectra are shown near their peak brightness. Vertical lines indicate prominent spectral features in ANTs. The spectra are offset for visual clarity.

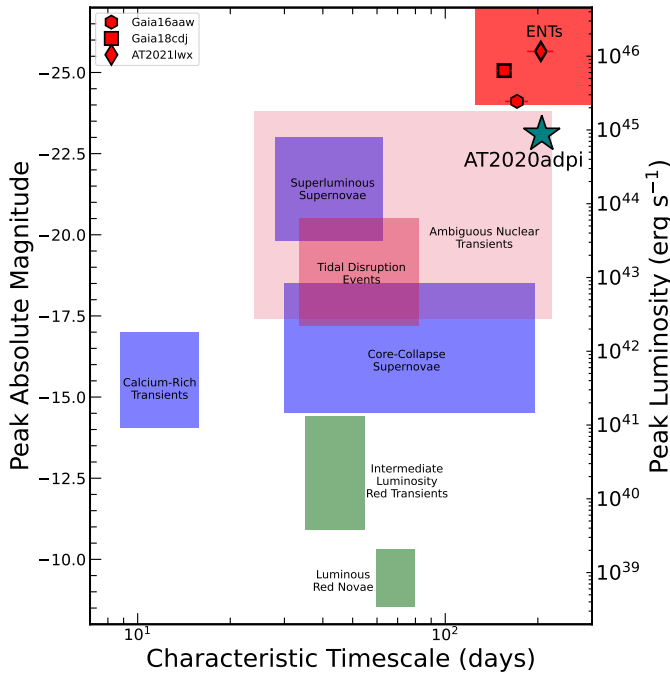


FIG. 8.— Comparison of AT2020adpi with other known transients in the optical absolute magnitude versus characteristic timescale parameter space, adapted from Hinkle et al. (2025). The blue-shaded regions represent various classes of SNe, green regions correspond to stellar mergers and/or mass transfer events, and red-shaded regions indicate transients powered by accretion onto SMBHs. The sample of ENTs described in Hinkle et al. (2025) is marked in red symbols. AT2020adpi shares features similar to ANTs and ENTs.

($f_c = 0.29$; Hinkle 2024b), and significantly higher than the values found in optically selected TDEs. Similar ambiguous cases include PS1-10adi (Kankare et al. 2017), ZTF18aajupnt (Frederick et al. 2019), ASASSN-18jd (Neustadt et al. 2020), and ASASSN-20hx (Hinkle et al. 2022a), all of which show mixed TDE/AGN traits.

Figure 8 places AT2020adpi within the broader distribution of nuclear transients, based on the typical peak absolute magnitude and the time it takes to fade to half of its peak luminosity of each class. Its location in the upper-right region of this diagram corresponds to events with high total radiated energy. In this context, many of AT2020adpi’s properties align with those seen in other ANTs. The rise time is also consistent with those of the ANTs (Wiseman et al. 2025).

The increasing sample of ANTs highlights the challenge of classification in the era of wide-field time-domain surveys and enhances the need for multi-wavelength, spectroscopic, and long-term monitoring to disentangle their physical origins. We anticipate finding more such events with the Rubin LSST survey, which will help us decipher their light curves, spectra, and host galaxy properties.

ACKNOWLEDGEMENTS

We thank the Swift observatory team for promptly scheduling and executing our TOO observations. PP thanks Rick Pogge for valuable comments on the KCWI spectrum and the Transients from Space Workshop participants at STScI for helpful suggestions and discussions. CSK is supported by NSF grants AST-2307385 and AST-2407206. Parts of this research were supported by the Australian Research Council Discovery Early Career Researcher Award (DECRA) through project number DE230101069.

REFERENCES

- Adelman-McCarthy J. K., et al., 2006, *ApJS*, 162, 38
- Andrillat Y., 1968, *AJ*, 73, 862
- Arcavi I., et al., 2014, *ApJ*, 793, 38
- Auchettl K., Guillochon J., Ramirez-Ruiz E., 2017, *ApJ*, 838, 149
- Auchettl K., Ramirez-Ruiz E., Guillochon J., 2018, *ApJ*, 852, 37
- Baldwin J. A., Ferland G. J., Korista K. T., Hamann F., LaCluyze A., 2004, *The Astrophysical Journal*, 615, 610–624
- Bellm E. C., et al., 2019a, *PASP*, 131, 018002
- Bellm E. C., et al., 2019b, *PASP*, 131, 018002
- Bianchi S., Guainazzi M., Matt G., Chiaberge M., Iwasawa K., Fiore F., Maiolino R., 2005, *A&A*, 442, 185
- Blagorodnova N., et al., 2017, *ApJ*, 844, 46
- Blanchard P. K., et al., 2017, *ApJ*, 843, 106
- Bose S., et al., 2018, *ApJ*, 853, 57
- Breeveld A. A., et al., 2010, *MNRAS*, 406, 1687
- Brown J. S., et al., 2018, *MNRAS*, 473, 1130
- Bruzual G., Charlot S., 2003, *MNRAS*, 344, 1000
- Cardelli J. A., Clayton G. C., Mathis J. S., 1989, *ApJ*, 345, 245
- Chambers K. C., et al., 2016, preprint, (arXiv:1612.05560)
- Charalampopoulos P., et al., 2022, *Astronomy & Astrophysics*, 659, A34
- Chu M., Dahiwalé A., Fremling C., 2021a, Transient Name Server Classification Report, 2021-2580, 1
- Chu M., Dahiwalé A., Fremling C., 2021b, Transient Name Server Classification Report, 2021-2580, 1
- Cushing M. C., Vacca W. D., Rayner J. T., 2004, *PASP*, 116, 362
- Dai L., McKinney J. C., Roth N., Ramirez-Ruiz E., Miller M. C., 2018, *ApJ*, 859, L20
- Denney K. D., Peterson B. M., Dietrich M., Vestergaard M., Bentz M. C., 2009, *ApJ*, 692, 246
- Dickey J. M., Lockman F. J., 1990, *ARA&A*, 28, 215
- Dong X.-B., Ho L. C., Wang J.-G., Wang T.-G., Wang H., Fan X., Zhou H., 2010, *ApJ*, 721, L143
- Dong S., et al., 2016, *Science*, 351, 257
- Draine B. T., 2011, Physics of the Interstellar and Intergalactic Medium
- Drake A. J., et al., 2009, *ApJ*, 696, 870
- Earl N., et al., 2025, astropy/specutils: v1.20.1, doi:10.5281/zenodo.15358062, https://doi.org/10.5281/zenodo.15358062
- Evans C. R., Kochanek C. S., 1989, *ApJ*, 346, L13
- Frederick S., et al., 2019, *ApJ*, 883, 31
- Frederick S., et al., 2020, arXiv e-prints, p. arXiv:2010.08554
- French K. D., Arcavi I., Zabludoff A., 2016, *ApJ*, 818, L21
- Gaia Collaboration et al., 2021, *A&A*, 649, A1
- Gaskell C. M., Rojas Lobos P. A., 2014, *MNRAS*, 438, L36
- Gezari S., et al., 2012, *Nature*, 485, 217
- Gezari S., Cenko S. B., Arcavi I., 2017a, *ApJ*, 851, L47
- Gezari S., Cenko S. B., Arcavi I., 2017b, *ApJ*, 851, L47
- Godoy-Rivera D., et al., 2017, *MNRAS*, 466, 1428
- Graham M. J., et al., 2019, *PASP*, 131, 078001
- Gromadzki M., et al., 2019, *A&A*, 622, L2
- Guillochon J., Ramirez-Ruiz E., 2013, *ApJ*, 767, 25
- Guo W.-J., et al., 2025, *ApJS*, 278, 28
- HI4PI Collaboration et al., 2016, *A&A*, 594, A116
- Hammerstein E., et al., 2023, Integral Field Spectroscopy of 13 Tidal Disruption Event Hosts from the ZTF Survey (arXiv:2307.15705), https://arxiv.org/abs/2307.15705
- Hinkle J. T., 2024a, *MNRAS*, 531, 2603
- Hinkle J. T., 2024b, *MNRAS*, 531, 2603
- Hinkle J. T., et al., 2021a, *MNRAS*, 500, 1673
- Hinkle J. T., Holoién T. W. S., Shappee B. J., Auchettl K., 2021b, *ApJ*, 910, 83
- Hinkle J. T., et al., 2022b, *The Astrophysical Journal*, 930, 12
- Hinkle J. T., et al., 2022a, *ApJ*, 930, 12
- Hinkle J. T., Shappee B. J., Holoién T. W. S., 2024, *MNRAS*, 528, 4775
- Hinkle J. T., et al., 2025, *Science Advances*, 11, ead10074
- Holoién T. W. S., et al., 2014a, *MNRAS*, 445, 3263
- Holoién T. W. S., et al., 2014b, *ApJ*, 785, L35
- Holoién T. W. S., et al., 2016a, *MNRAS*, 455, 2918
- Holoién T. W. S., et al., 2016b, *MNRAS*, 455, 2918
- Holoién T. W. S., et al., 2016c, *MNRAS*, 463, 3813
- Holoién T. W. S., et al., 2019a, *MNRAS*, 484, 1899
- Holoién T. W. S., et al., 2019b, *ApJ*, 880, 120
- Holoién T. W. S., et al., 2019c, *ApJ*, 880, 120
- Holoién T. W. S., et al., 2019d, *ApJ*, 883, 111
- Holoién T. W. S., et al., 2020, arXiv e-prints, p. arXiv:2003.13693
- Holoién T. W. S., et al., 2022, *The Astrophysical Journal*, 933, 196
- Hoogendam W. B., et al., 2024, *Monthly Notices of the Royal Astronomical Society*, 530, 4501–4518
- Hung T., et al., 2017, *ApJ*, 842, 29
- Hung T., et al., 2020a, arXiv e-prints, p. arXiv:2003.09427
- Hung T., et al., 2020b, arXiv e-prints, p. arXiv:2011.01593
- Hwang H.-C., Zakamska N. L., 2020, *MNRAS*, 493, 2271
- Jones D. O., et al., 2021, *ApJ*, 908, 143
- Kalberla P. M. W., Burton W. B., Hartmann D., Arnal E. M., Bajaja E., Morras R., Pöppel W. G. L., 2005, *A&A*, 440, 775
- Kankare E., et al., 2017, *Nature Astronomy*, 1, 865
- Kochanek C. S., 2016, *MNRAS*, 461, 371
- Kochanek C. S., et al., 2017, *PASP*, 129, 104502
- Komossa S., et al., 2024, arXiv e-prints, p. arXiv:2408.00089
- Koratkar A., Blaes O., 1999, *PASP*, 111, 1
- Kriek M., van Dokkum P. G., Labbé I., Franx M., Illingworth G. D., Marchesini D., Quadri R. F., 2009, *ApJ*, 700, 221
- Lantz B., et al., 2004, in Mazuray L., Rogers P. J., Wartmann R., eds, Proc. SPIE Vol. 5249, Optical Design and Engineering. pp 146–155, doi:10.1117/12.512493
- Leloudas G., et al., 2016, *Nature Astronomy*, 1, 0002
- Leloudas G., et al., 2019a, arXiv e-prints,
- Leloudas G., et al., 2019b, *The Astrophysical Journal*, 887, 218
- López-Gonzaga N., Burtscher L., Tristram K. R. W., Meisenheimer K., Schartmann M., 2016, *Astronomy & Astrophysics*, 591, A47
- MacLeod C. L., et al., 2010, *ApJ*, 721, 1014
- MacLeod C. L., et al., 2012, *ApJ*, 753, 106
- MacLeod C. L., et al., 2016, *MNRAS*, 457, 389
- MacLeod C. L., et al., 2019, *ApJ*, 874, 8
- Mainzer A., et al., 2011, *ApJ*, 743, 156
- Makrygianni L., et al., 2023, *The Astrophysical Journal*, 953, 32
- Masci F. J., et al., 2023, A New Forced Photometry Service for the Zwicky Transient Facility (arXiv:2305.16279), https://arxiv.org/abs/2305.16279
- McConnell N. J., Ma C.-P., 2013, *ApJ*, 764, 184
- Mockler B., Ramirez-Ruiz E., 2021, *The Astrophysical Journal*, 906, 101
- Mockler B., Melchor D., Naoz S., Ramirez-Ruiz E., 2023, *ApJ*, 959, 18
- Neustadt J. M. M., et al., 2020, *MNRAS*, 494, 2538
- Nicholl M., et al., 2016, *ApJ*, 826, 39
- Nicholl M., et al., 2020, arXiv e-prints, p. arXiv:2006.02454
- Oke J. B., et al., 1995, *PASP*, 107, 375
- Oknyanskij V. L., 1978, *Peremennye Zvezdy*, 21, 71
- Osterbrock D. E., Pogge R. W., 1985, *ApJ*, 297, 166
- Padovani P., et al., 2017, *A&A Rev.*, 25, 2
- Paolillo M., Papadakis I., 2025, arXiv e-prints, p. arXiv:2506.23899
- Peterson B. M., 1997, An Introduction to Active Galactic Nuclei
- Peterson B. M., et al., 2004, *ApJ*, 613, 682
- Phinney E. S., 1989, *Nature*, 340, 595
- Poole T. S., et al., 2008, *MNRAS*, 383, 627
- Prochaska J. X., et al., 2020a, pypeit/Pypeit: Release 1.0.0, doi:10.5281/zenodo.3743493
- Prochaska J. X., Hennawi J. F., Westfall K. B., Cooke R. J., Wang F., Hsu T., Davies F. B., Farina E. P., 2020b, arXiv e-prints, p. arXiv:2005.06505
- Prochaska J. X., et al., 2020c, *Journal of Open Source Software*, 5, 2308
- Rayner J. T., Toomey D. W., Onaka P. M., Denault A. J., Stahlberger W. E., Vacca W. D., Cushing M. C., Wang S., 2003, *PASP*, 115, 362
- Rees M. J., 1988, *Nature*, 333, 523
- Ricci C., Trakhtenbrot B., 2023, *Nature Astronomy*, 7, 1282
- Ricci C., et al., 2017, *ApJS*, 233, 17
- Ricci C., et al., 2020, *ApJ*, 898, L1
- Roth N., Kasen D., 2018, *ApJ*, 855, 54
- Roth N., Kasen D., Guillochon J., Ramirez-Ruiz E., 2016, *ApJ*, 827, 3
- Salpeter E. E., 1955, *ApJ*, 121, 161
- Schlafly E. F., Finkbeiner D. P., 2011, *ApJ*, 737, 103
- Shappee B. J., et al., 2014, *ApJ*, 788, 48
- Shappee B. J., et al., 2016, *ApJ*, 826, 144
- Shen Y., Kelly B. C., 2012, *ApJ*, 746, 169
- Sheng Z., Wang T., Jiang N., Yang C., Yan L., Dou L., Peng B., 2017, *ApJ*, 846, L7
- Sheng Z., et al., 2020, *ApJ*, 889, 46
- Strateva I. V., Brandt W. N., Schneider D. P., Vanden Berk D. G., Vignali C., 2005, *The Astronomical Journal*, 130, 387–405
- Strubbe L. E., Murray N., 2015, *MNRAS*, 454, 2321
- Subrayan B. M., et al., 2023, *The Astrophysical Journal Letters*, 948, L19
- Tadhunter C., Spence R., Rose M., Mullaney J., Crowther P., 2017, *Nature Astronomy*, 1, 0061
- Temple M. J., et al., 2023, *MNRAS*, 523, 646
- Tohline J. E., Osterbrock D. E., 1976, *ApJ*, 210, L117
- Tony J. L., et al., 2018, *PASP*, 130, 064505
- Trakhtenbrot B., et al., 2019a, *Nature Astronomy*, 3, 242
- Trakhtenbrot B., et al., 2019b, *ApJ*, 883, 94
- Trakhtenbrot B., et al., 2019c, *ApJ*, 883, 94
- Tucker M. A., et al., 2022, *Publications of the Astronomical Society of the Pacific*, 134, 124502
- Vanden Berk D. E., et al., 2001, *AJ*, 122, 549
- Wang J.-G., et al., 2009, *The Astrophysical Journal*, 707, 1334–1346
- Wevers T., 2020, *MNRAS*, 497, L1
- Wevers T., et al., 2019a, *MNRAS*, 488, 4816
- Wevers T., et al., 2019b, *MNRAS*, 488, 4816
- Wiseman P., et al., 2023, *MNRAS*, 522, 3992
- Wiseman P., et al., 2025, *MNRAS*, 537, 2024
- Wright E. L., 2006, *PASP*, 118, 1711
- Yan L., et al., 2019, *ApJ*, 874, 44

Yao Y., et al., 2023, [ApJ](#), 955, L6
Zu Y., Kochanek C. S., Peterson B. M., 2011, [ApJ](#), 735, 80
van Velzen S., et al., 2016, [Science](#), 351, 62

van Velzen S., Gezari S., Hung T., Gatkine P., Cenko S. B., Ho A., Kulkarni S. R., Mahabal A., 2019, [The Astronomer's Telegram](#), 12568, 1
van Velzen S., et al., 2021, [ApJ](#), 908, 4

This paper was built using the Open Journal of Astrophysics \LaTeX template. The OJA is a journal which provides fast and easy peer review for new papers in the `astro-ph` section of the

arXiv, making the reviewing process simpler for authors and referees alike. Learn more at <http://astro.theoj.org>.